Supplementary Information

Highly stable inverted methylammonium lead tri-iodide perovskite solar cells achieved by surface re-crystallization

Hyungcheol Back[a,b‡], Geunjin Kim[a,c‡], Heejoo Kim[a,d*], Chang-Yong Nam[e], Jinhyun Kim[f], Yong-Ryun Kim[a], Taejin Kim[g], Byoungwook Park[g], James R. Durrant[f], Kwanghee Lee[a,h*]

[a]Heeger Center for Advanced Materials & Research Institute for Solar and Sustainable Energies, Gwangju Institute of Science and Technology, Gwangju 61005, Republic of Korea, [b]Hanwha Q Cells & Advanced Materials, 305 Pangyo-ro, Bundanggu, Seongnam, Gyeonggi 13488, Republic of Korea, [c]Division of Advanced Materials, Korea Research Institute of Chemical Technology, 141 Gajeong-Ro, Yuseong-Gu, Daejeon 34114, Republic of Korea, [d]Institute of Integrated Technology, Gwangju Institute of Science and Technology, Gwangju 61005, Republic of Korea, [e]Center for Functional Nanomaterials, Brookhaven National Laboratory, Upton, New York 11973, USA, [f]Department of Chemistry and Centre for Plastic Electronics, Imperial College London, London SW7 2AZ, United Kingdom, [g]Department of Materials Science and Chemical Engineering, Stony Brook University, Stony Brook, New York 11794, USA, [h]School of Materials Science and Engineering, Gwangju Institute of Science and Technology, Gwangju 61005, Republic of Korea.

[‡]H. Back and G. Kim contributed equally to this work.

[*]To whom correspondence should be addressed: heejook@gist.ac.kr (H.Kim), klee@gist.ac.kr (K. Lee)

Methods

Material Preparation. PTAA and PFN were purchased from EM Index and 1-Material and dissolved in toluene and anhydrous methanol (99.8%, Sigma-Aldrich) to 0.25 and 0.05 wt%, respectively. Lead (II) iodide (PbI_2) and MAI (CH_3NH_3I) were purchased from Alfa Aesar and GreatCell Solar, respectively. A 1.5 M perovskite precursor solution was prepared by dissolving PbI_2 and CH_3NH_3I at a molar ratio of 1:1 in N,N-dimethylformamide and dimethyl sulfoxide mixed solution (9:1 v/v) at 60 °C overnight. PCBM purchased from Nano-C was dissolved in chlorobenzene (CB) with 4 wt%. Titanium (IV) isopropoxide (TTIP), 1,1-bis(diphenylphosphino)methane (DPPM), toluene, and isopropyl alcohol (IPA) were purchased from Sigma-Aldrich and used without redistillation. For preparation of the titanium suboxide (TiO_x) precursor solution, TTIP (100 µl) was added to a solution consisting of toluene (1 ml) and DPPM (63 mg), and the transparent precursor was diluted by IPA to a volume ratio of 1:30.

Device Fabrication. For the fabrication of the p-i-n planar heterojunction (PHJ)-type PeSCs, the PTAA solution was first spin-cast onto an ITO glass substrate at 5000 rpm for 40 s and then dried at 150 °C for 10 min under ambient conditions. The PFN solution was then spin-coated on the PTAA/ITO substrate at 5000 rpm for 30 s under ambient conditions. For deposition of the perovskite layers, the precursor solution was coated onto the PFN/PTAA/ITO substrate using a one-step spin-casting process at 5000 for 30 s. After 5 s during the spin-casting process, the perovskite layer was treated with 0.5 ml of diethyl ether (Sigma-Aldrich) by drop-casting and then annealed at 100 °C for 10 min. Afterward, a solution containing 4 wt% PCBM in CB was spin-casted at 1500 rpm for 40 s, and then, the PCBM/perovskite/PFN/PTAA/ITO sample was maintained under high vacuum (10^{-6} mbar) for 100 hours. Afterward, the PCBM layer was washed off with 1 ml of toluene, and PCBM was redeposited using the same conditions. The TiO_x solution was spin-coated at 5000 rpm for 30 s and dried at 100 °C for 5 min. Finally, the p-i-n PHJ devices were completed by evaporating a copper (Cu) electrode through a shadow mask under high vacuum (10^{-6} mbar).
For the fabrication of the electron-only devices, a C_{60} (Nano-C) layer (40 nm) was vacuum deposited onto an ITO glass substrate under high vacuum (10^{-6} mbar). For deposition of the perovskite layers in the N_2-filled glove box, the precursor solution was coated onto the C_{60}/ITO substrate using a one-step spin-casting process at 5000 for 30 s. After 5 s during the spin-casting process, the perovskite layer was treated with 0.5 ml of diethyl ether by drop-casting and then dried at 100 °C for 10 min. Afterward, a solution containing 4 wt% PCBM in chlorobenzene was spin-casted at 1500 rpm for 40 s, and then, the PCBM/perovskite/C_{60}/ITO sample was maintained under high vacuum (10^{-6} mbar) for 100 hours. Afterward, the PCBM layer was washed off with 1 ml of toluene, and PCBM was redeposited using the same conditions. TiO_x was spin-coated at 5000 rpm for 30 s and dried at 100 °C for 5 min. Finally, the electron-only devices were completed by evaporating an aluminum electrode through a shadow mask under high vacuum (10^{-6} mbar).

Characterization. The current density-voltage (J-V) characteristics (in the range of -0.2 V to 1.2 V) of the unit cells (with a metal aperture of an area of 4.64 mm^2) were measured using a Keithley 238 source measure unit (Keithley Instruments, Inc., Cleveland, OH, USA) with 10 ms delay under air mass 1.5 global (AM 1.5G) simulated solar illumination emitted at 100 mW cm^{-2} from a Newport 750 solar simulator. IPCE measurements of the PHJ PeSCs were performed using a Solar

Cell Spectral Response/QE/IPCE measuring system (PV Measurements, Inc., Boulder, CO, USA). XPS measurements were performed on a VG Multilab 2000 under high vacuum (10^{-9} mbar). The XPS spectra were calibrated by the binding energy of 285 eV for C 1s. Scanning electron microscopy (SEM) images were captured with a Hitachi S-4700 instrument.

XPS compositional depth profiling was performed at the Center for Functional Nanomaterials, Brookhaven National Laboratory, using an ultrahigh vacuum (UHV, with base pressures < 2 x 10-9 Torr) multiprobe surface analysis system equipped with a hemispherical electron energy analyzer (SPECS, PHOIBOS 100) and a twin anode X-ray source (SPECS, pXR50, Al Kα (1486.6 eV)). Depth profiling of the composition and chemical states was performed by alternatively repeating XPS analysis and surface layer removal. The surface layer (5 mm x 5 mm area) was removed by timed Ar+ ion beam (2 kV) sputtering.

GIWAXS measurements were performed at the CMS (11-BM) beamline of the National Synchrotron Light Source II at Brookhaven National Laboratory. An X-ray (13.5 keV, $\lambda = 0.918$ Å) beam with a footprint of 0.150 mm × 0.150 mm (defined by a slit) was irradiated on samples in vacuum (~100 mTorr) for 10 s with the incidence angle varying from 0.08° to 0.4°. GIWAXS data collections were performed on two different locations with four incident angles, from 0.08, 0.1, 0.2, 0.3, and 0.4 degrees (thus total 10 separate measurements in each sample). All three samples for each scenario had the identical visual appearance (i.e., size (1.5 cm × 1.5 cm), roughness, and color of films) which is translated to nearly identical device characteristics based on our extensive, repeated device experiments. The X-ray scattering signal was collected using a fiber-coupled CCD area detector (Photonic Sciences, ImageStar), covering a q-range from 0.12 $Å^{-1}$ to 4.09 $Å^{-1}$. The data were analyzed using SciAnalysis (http://gisaxs.com/index.php/SciAnalysis).

The IS measurements were performed in the galvanostat mode (PGSTAT30, AutoLab, EcoChemie) under open-circuit conditions with various light intensities (e.g., a voltage of 1.07 V under AM 1.5G simulated solar illumination emitted at 100 mW cm^{-2} from a Newport 750 solar simulator). Transient photovoltage (TPV) measurements were performed by connecting the PeSCs, ITO/PTAA/PFN/perovskite/neat PCBM or VCRP/TiO_x/Cu across a 1 MΩ terminal of an oscilloscope (TDS520, Tektronix). A 6 ns optical pulse from the frequency-doubled outputs of a 532 nm Nd:YAG laser (LOTIS) and 1 mW cm^{-2} of continuous white light irradiation (0.01 sun) was applied. The resulting voltage transient was measured using the oscilloscope. Time-correlated single photon counting (TCSPC) measurement of the neat perovskite/PCBM and VCRP films on glass substrate was conducted by using DeltaFlex TSCPC system (Horiba Scientific, Japan) single-photon counting detector (PPD-900, Horiba scientific, Japan). The excitation source for TSCPC was a 635 nm diode laser (NanoLED N-02B, Horiba scientific, Japan) with a < 200 ps pulse duration and a 1 MHz repetition rate. To modulate the excitation pulse energy (< 1 nJ cm^{-2}), neutral density filters were used.

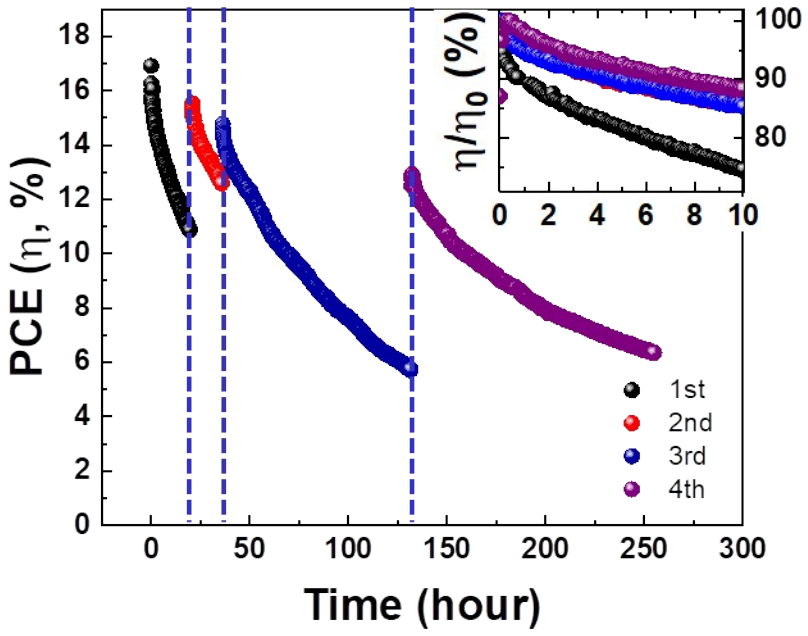

Supplementary Figure 1. The operational stability of pristine PeSCs according to the MPPT number.

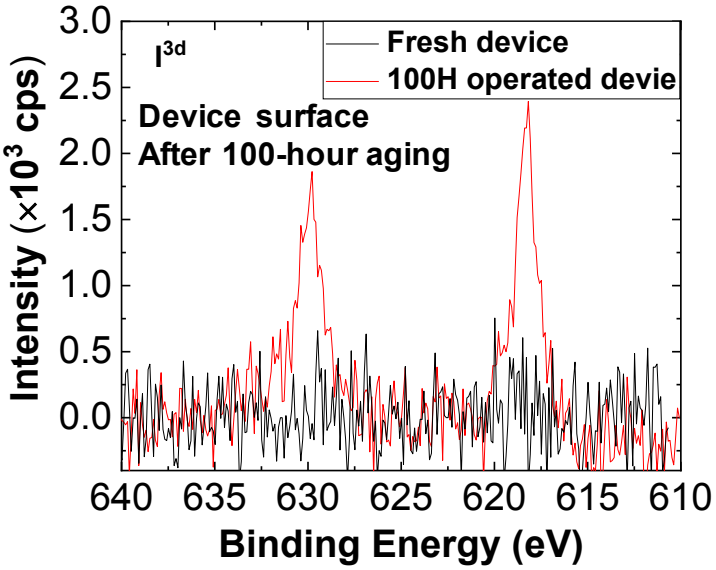

Supplementary Figure 2. Ion diffusion on the surface of the 100-hour aged device.

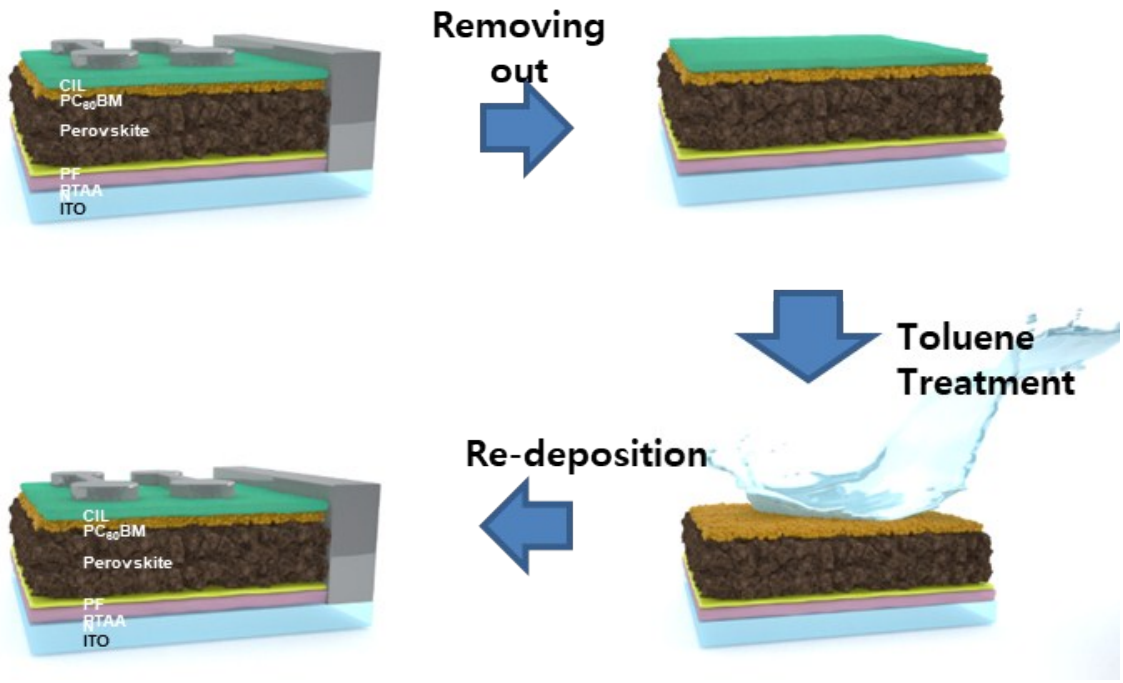

Supplementary Figure 3. Schematic diagram of the regeneration of PeSCs.

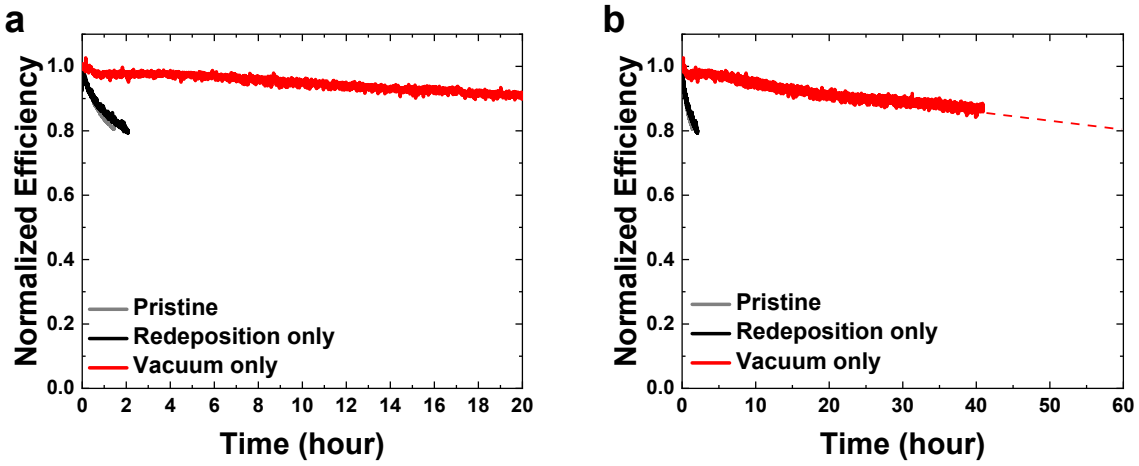

Supplementary Figure 4. The operational stability of pristine, PCBM redeposition, and vacuum only PeSCs.

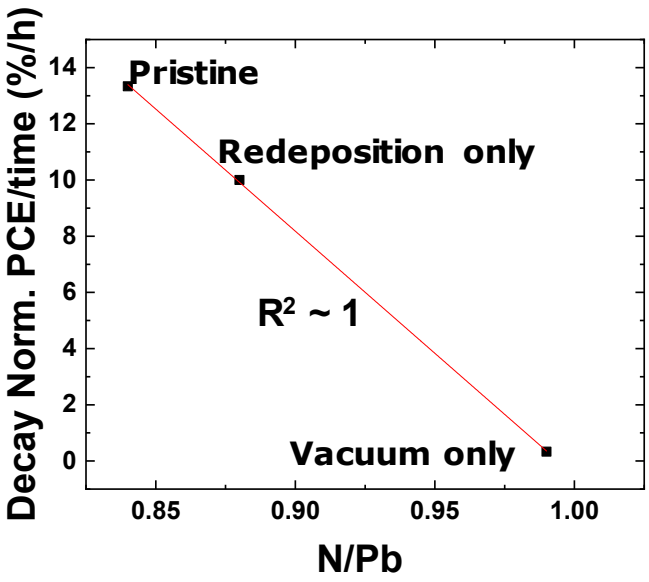

Supplementary Figure 5. The relation between N/Pb and fast burn-in decay rate for each case.

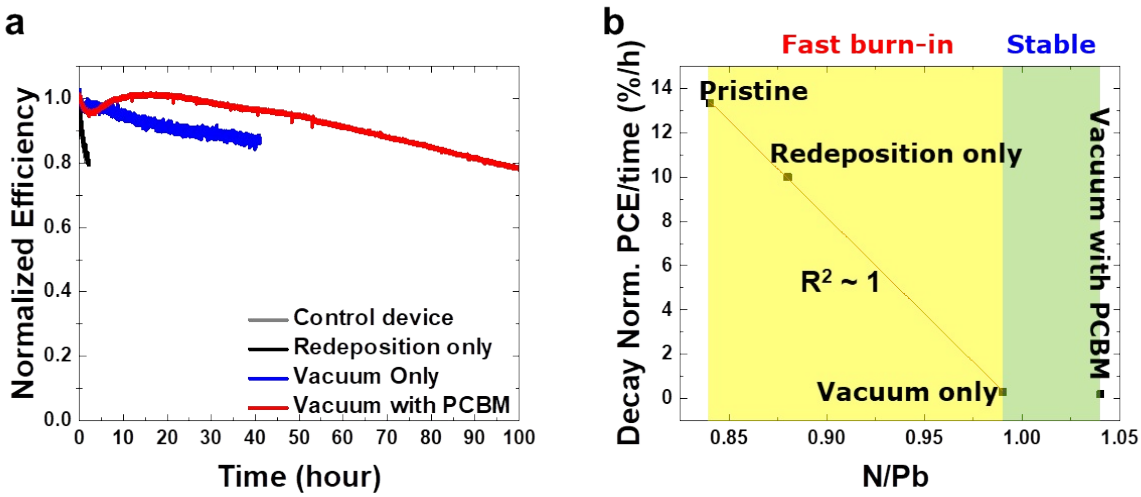

Supplementary Figure 6. The operational stability of pristine, PCBM-redeposition-only, vacuum-only, and vacuum-with-PCBM PeSCs.

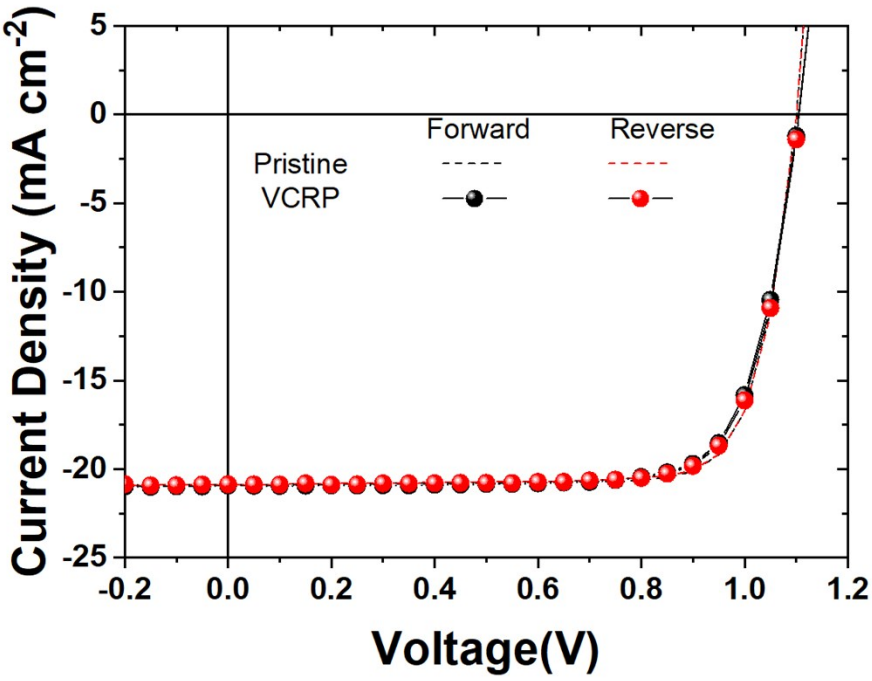

Supplementary Figure 7. J-V curve of pristine and VCRP PeSCs.

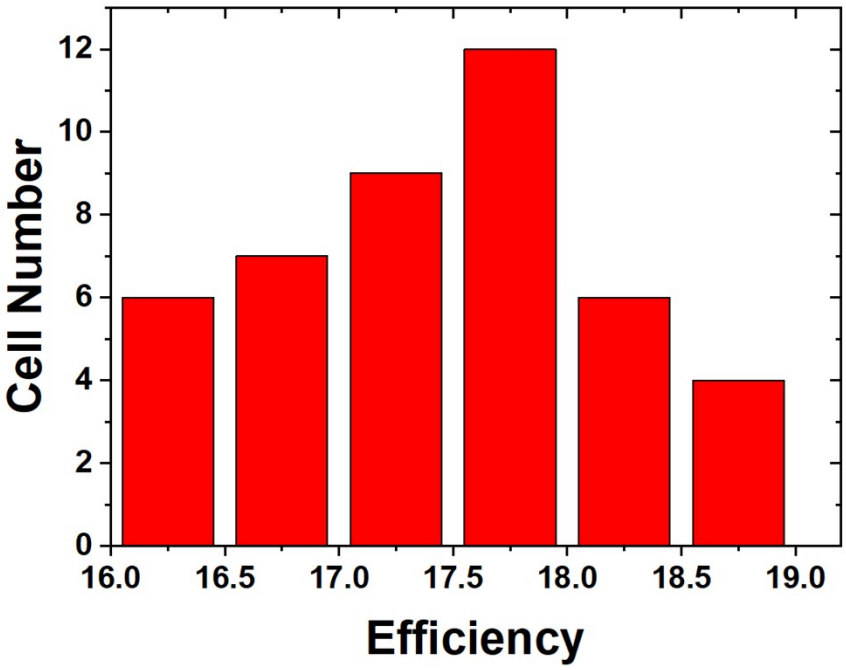

Supplementary Figure 8. Histogram of the average efficiencies of VCRP PeSCs.

General rules

- Measuring initial power density (V_0 & J_0 -> P_0=0 mW/cm^2)
- Up or down voltage (V_1) (V)
- Measuring current density (J_1) (mA/cm^2)
- Obtaining new power density P_1 (mW/cm^2)
- Comparing P_0 & P_1
- Change Voltage (w/ 0.01 V step)

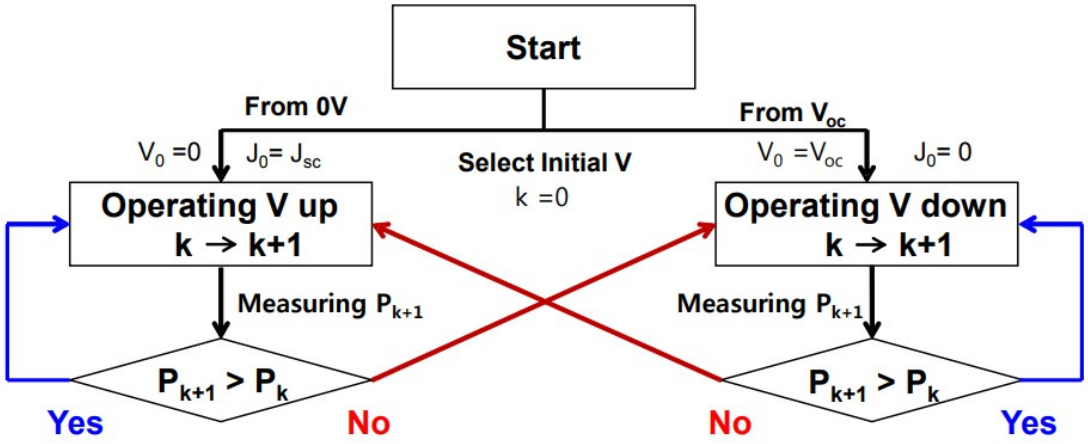

Supplementary Figure 9. Logic diagram of a perturb and observe (P&O) method for MPPT of the devices.

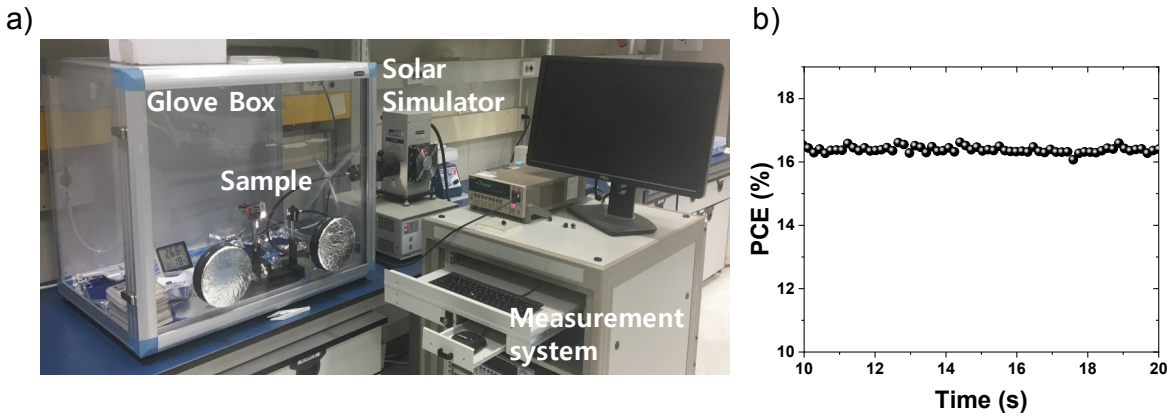

Supplementary Figure 10. (a) Picture of the MPPT measurement system and (b) MPPT of PeSCs for 20 s.

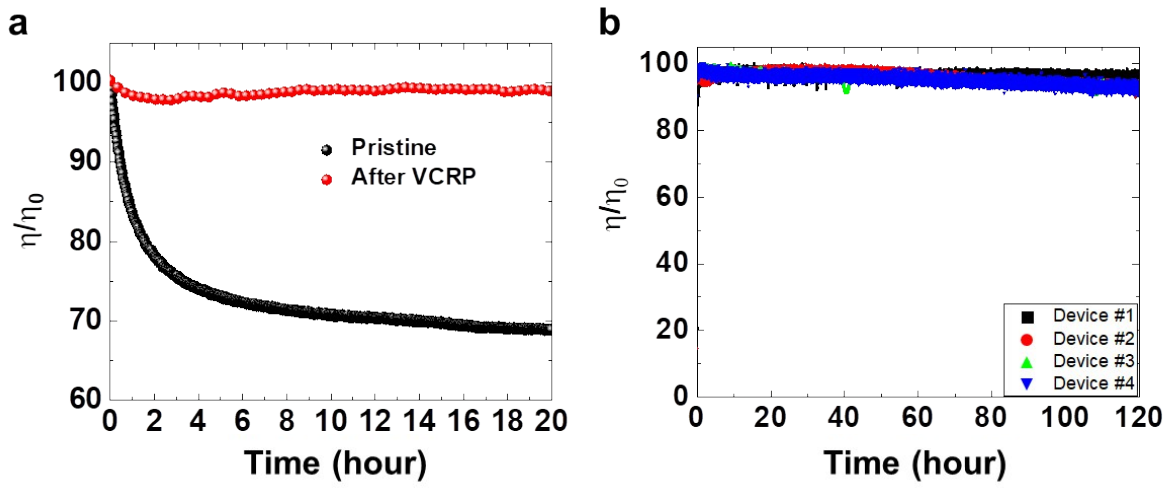

Supplementary Figure 11. **MPP tracking curves of pristine and VCRP PeSCs** (a) for 20 hours. (b) MPP tracking measurement of four VCRP processed PeSCs for 120 hours.

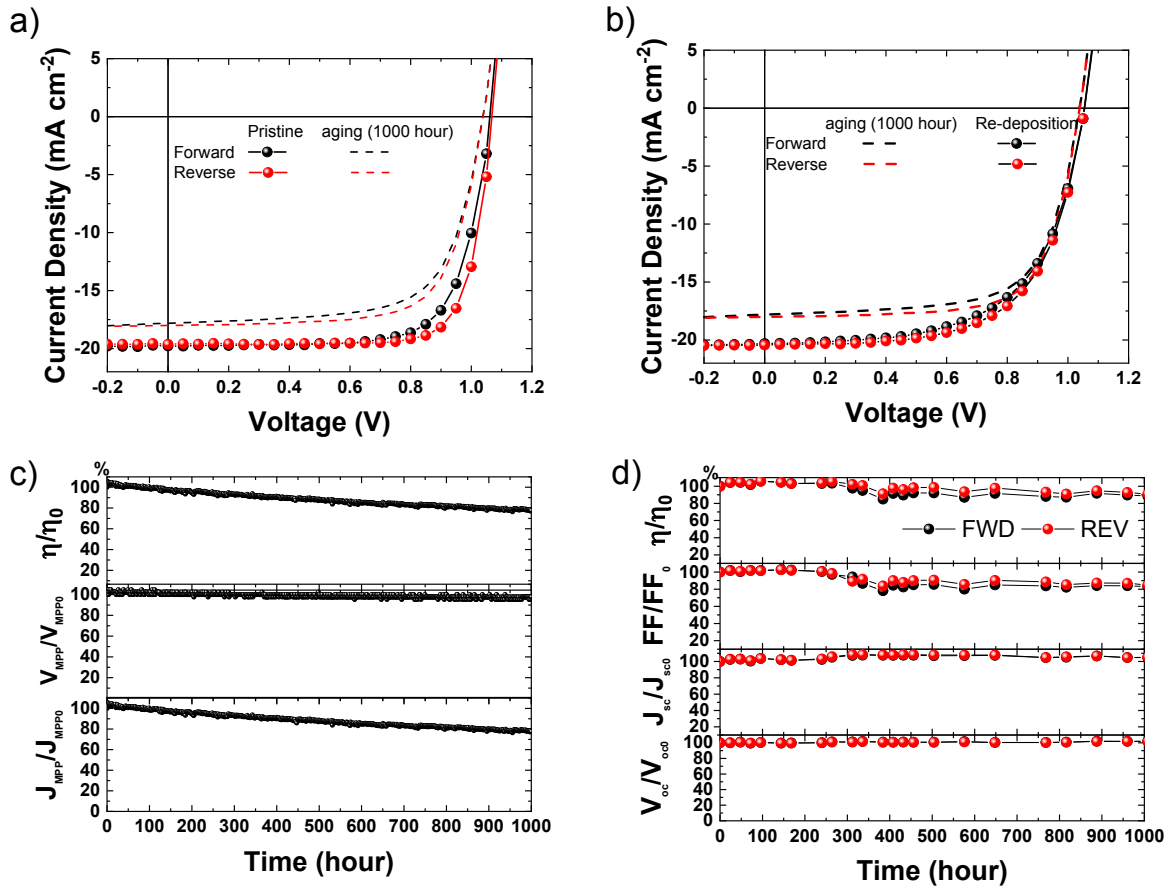

Supplementary Figure 12. (a) J-V characteristics of pristine and 1000-hours aged VCRP PeSCs and (b) aged and redeposited VCRP PeSCs. Comparison of stability of photovoltaic parameters of VCRP PeSCs under (c) continuous operation (AM 1.5G irradiation, inert N_2 gas condition) and (d) continuous heat condition (at 85 °C in the dark, inert N_2 gas condition).

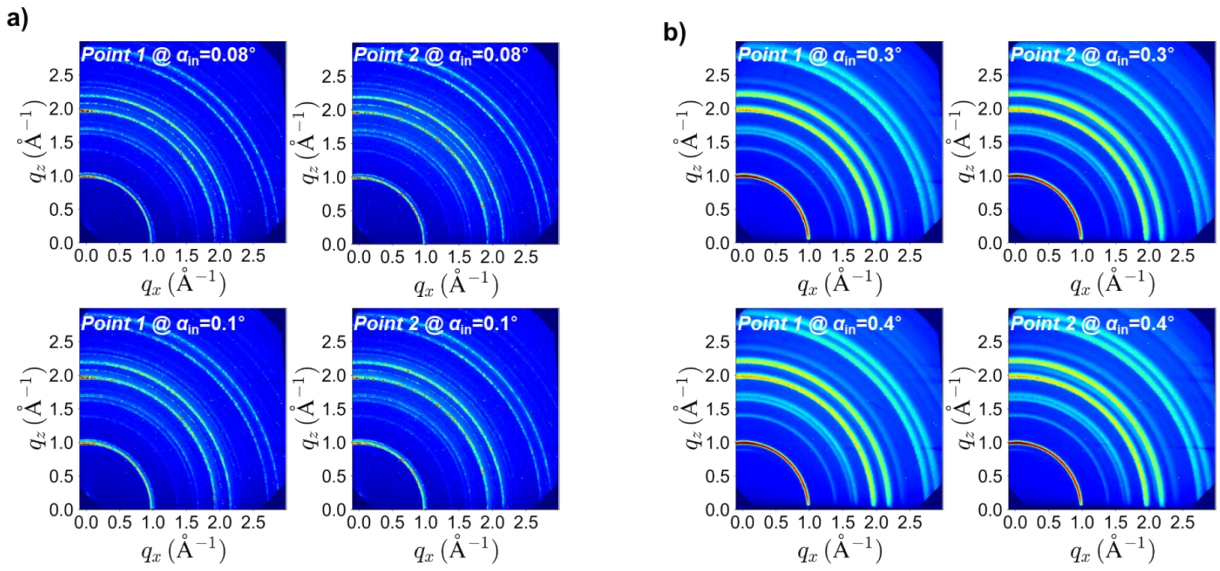

Supplementary Figure 13. 2-D GIWAXS patterns on with different measuring points at each incident angle indicating a) surface (incident angle: 0.08 and 0.1°) and b) bulk (incident angle: 0.3 and 0.4°) information.

Supplementary Note S1. For each sample, GIWAXS data collections were performed on two different locations with four incident angles, from 0.08, 0.1, 0.2, 0.3, and 0.4 degrees (thus total 10 separate measurements in each sample, the case of 0.2 ° was not shown). Given that the data from the incident angles of 0.08 and 0.1 predominantly deliver the surface information while those from 0.3 and 0.4 degrees the bulk information, we can state that the surface and bulk structures of a given sample were examined by four separate measurements, respectively. We find that these four separate measurements for a given condition yielded a consistent data (Supplementary Figure 10).

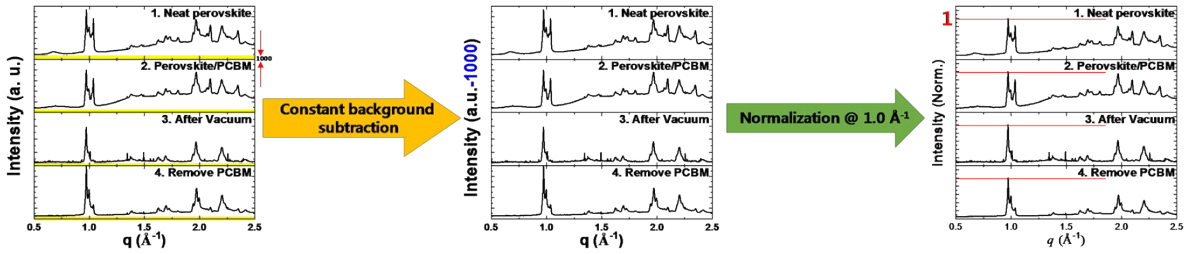

Supplementary Figure 14. **Rescaling procedure of circular average**

Supplementary Note 2. Penetration depth of X-ray

Previous X-ray studies indicate that the critical incidence angle in $MAPbI_3$ is ca. 0.16-0.3° at which the X-ray penetration depth is 140-150 nm (at 10 keV X-ray energy).[1-3] This confirms the low angle used in the present study (0.1°) is well below the reported critical angle, thus rendering this X-ray incidence primarily probing the top surface of $MAPbI_3$ film. We note that the calculation of exact X-ray penetration depth in $MAPbI_3$ for a given incidence angle and X-ray energy requires the X-ray linear attenuation coefficient of $MAPbI_3$, which is not available in the literatures. Below, we have estimated the penetration depth of 13 keV X-ray in $MAPbI_3$ film using the calculation table available at the SLAC National Laboratory website,[4] and following material parameters for $MAPbI_3$: Average atomic number of 21.667, molecular weight of 619.99 g mol^{-1}, and density (r) of 4.2846 g cm^{-3}. Since the X-ray linear attenuation coefficient of $MAPbI_3$ (m_{MAPI}) is not available, we assume Pb as the primary element that interacts with the incident X-ray and use the mass attenuation coefficient (M) of Pb (162.1 cm g^{-1}) available at the National Institute of Standards and Technology (NIST) database.[5] Subsequently, M can be converted to m_{MAPI} (ca. ~700 cm^{-1}) via its relationship with density (i.e., $m_{MAPI} = M \cdot r_{MAPI}$). Indeed, we estimate the penetration depth of 13 keV X-ray in $MAPbI_3$ film at 0.1° incidence angle to be ~23 nm and at 0.3° incidence angle to be ~74 nm (Supplementary Figure 15), confirming the validity of these used incident angles for studying the surface and bulk, respectively.

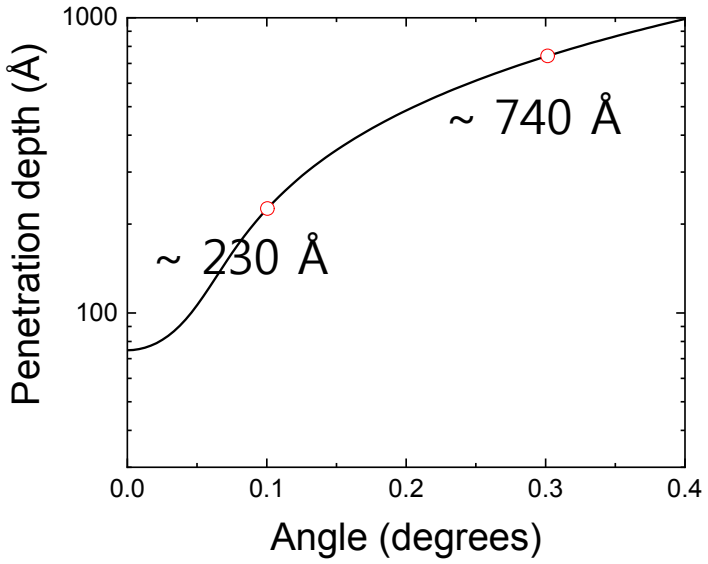

Supplementary Figure 15. Penetration depth of X-ray with incidence angle.

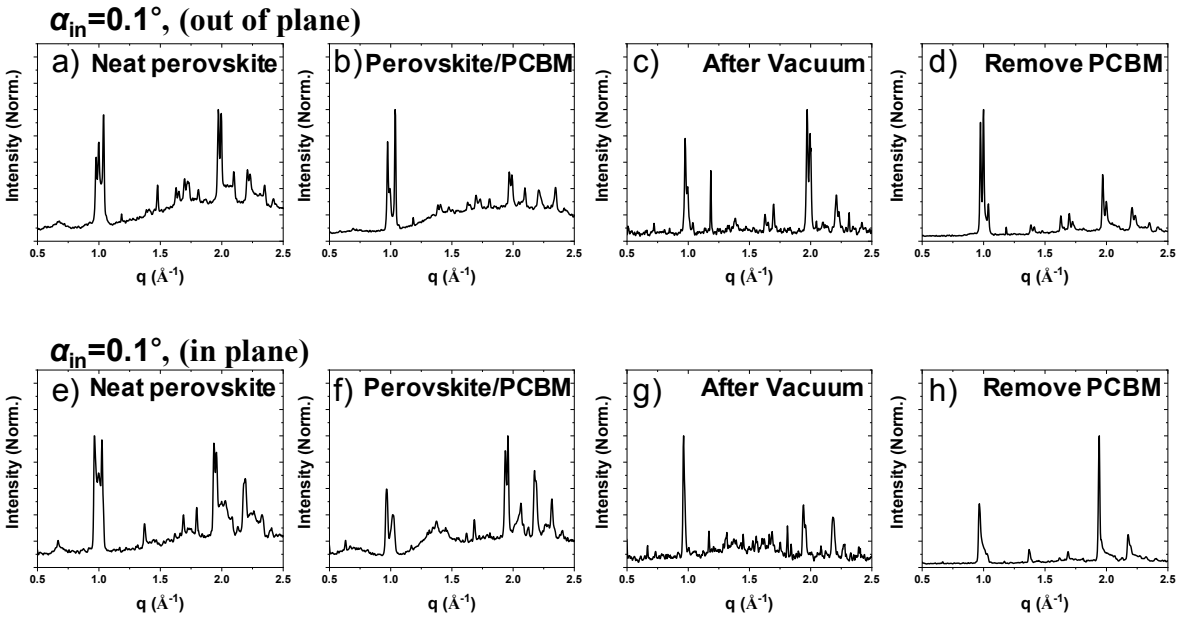

Supplementary Figure 16. Out-of-plane and in-plane surface crystallinity of (a, e) pristine perovskite, (b, f) perovskite layer with PCBM, and (c, g) perovskite layer with PCBM maintained under vacuum conditions for 100 hours and after (d, h) removal of PCBM.

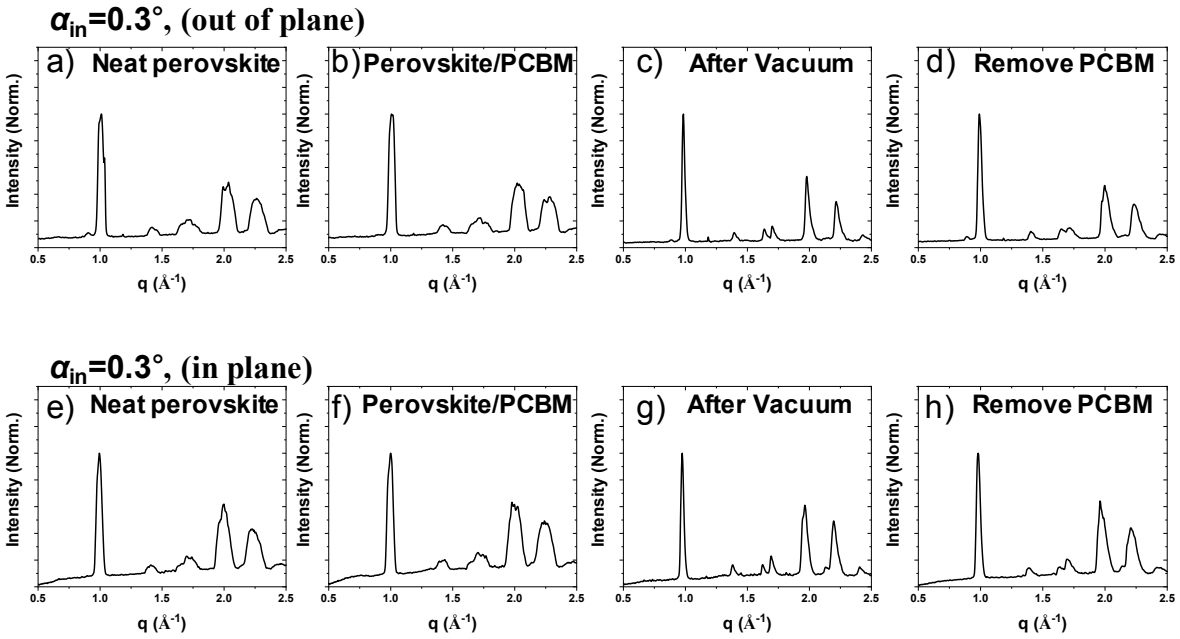

Supplementary Figure 17. Out-of-plane and in-plane bulk crystallinity of (a, e) pristine perovskite, (b, f) perovskite layer with PCBM, and (c, g) perovskite layer with PCBM maintained under vacuum conditions for 100 hours and after (d, h) removal of PCBM.

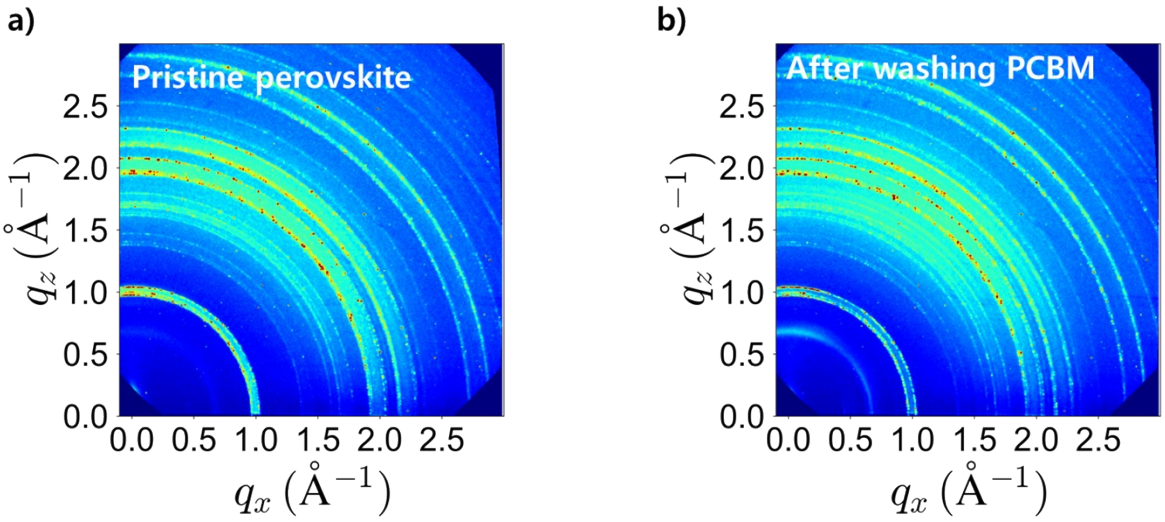

Supplementary Figure 18. GIWAXS data of perovskite films. (a) Pristine and (b) after washing PCBM.

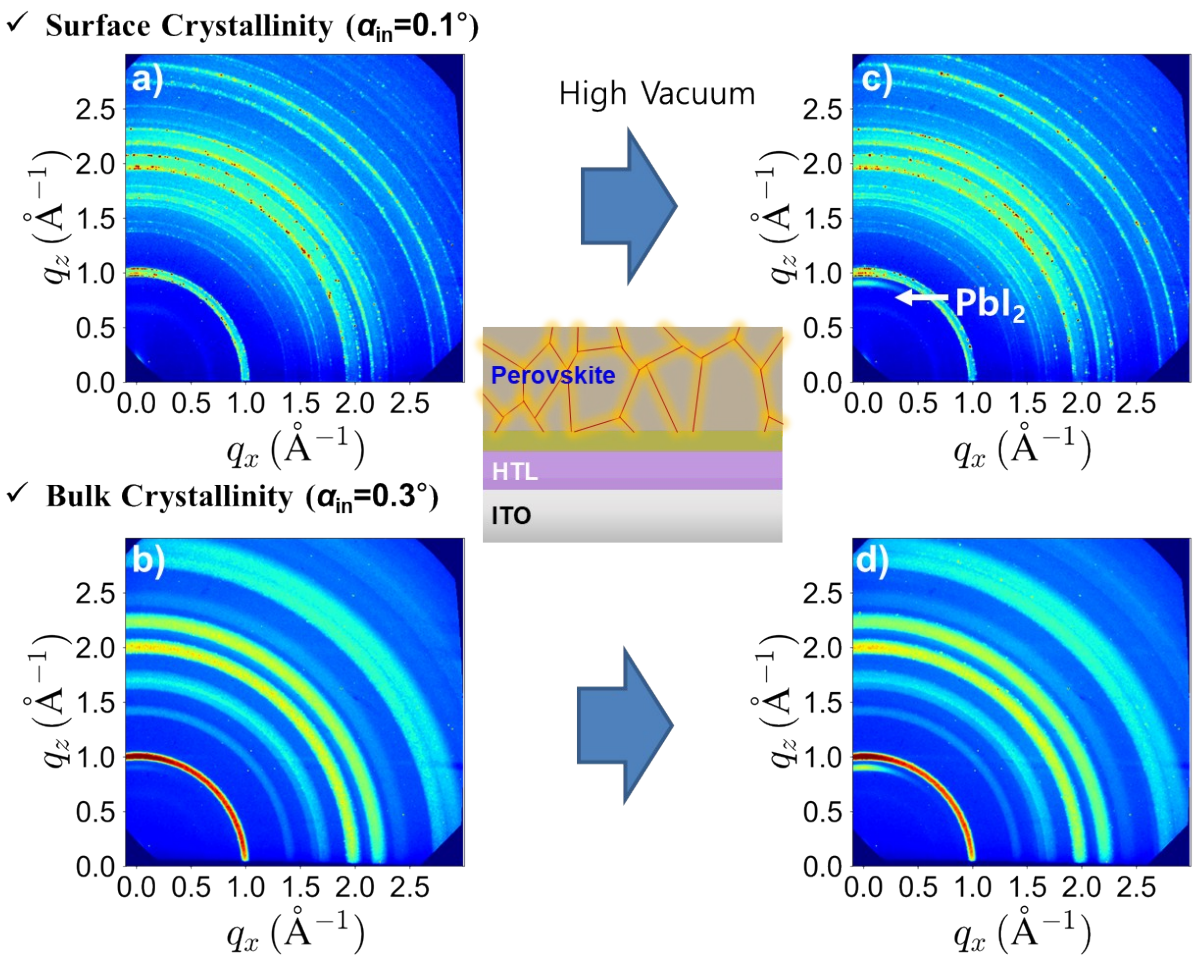

Supplementary Figure 19. 2-D GIWAXS image of surface and bulk crystallinity of (a, b) pristine perovskite and (c, d) perovskite layer maintained under vacuum conditions for 100 hours.

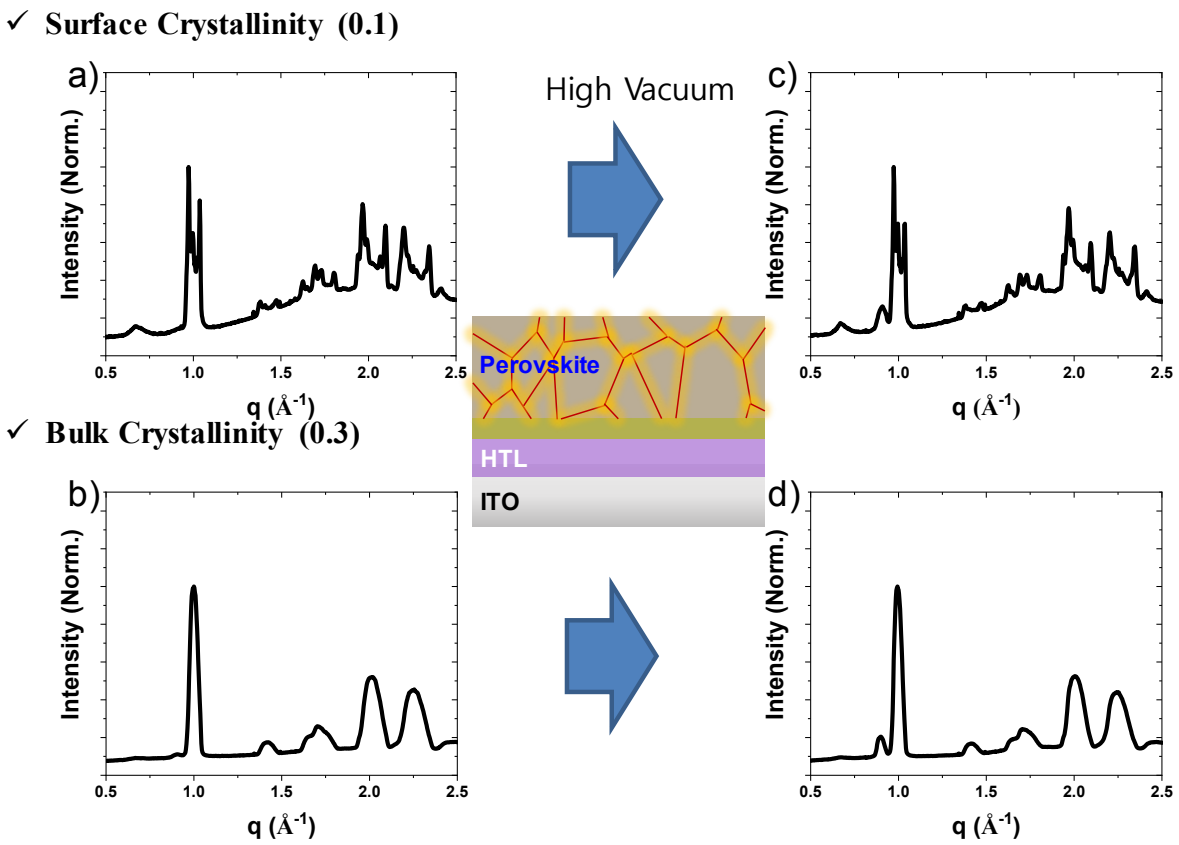

Supplementary Figure 20. Circular average of surface and bulk crystallinity of (a, b) pristine perovskite and (c, d) perovskite layer maintained under vacuum conditions for 100 hours.

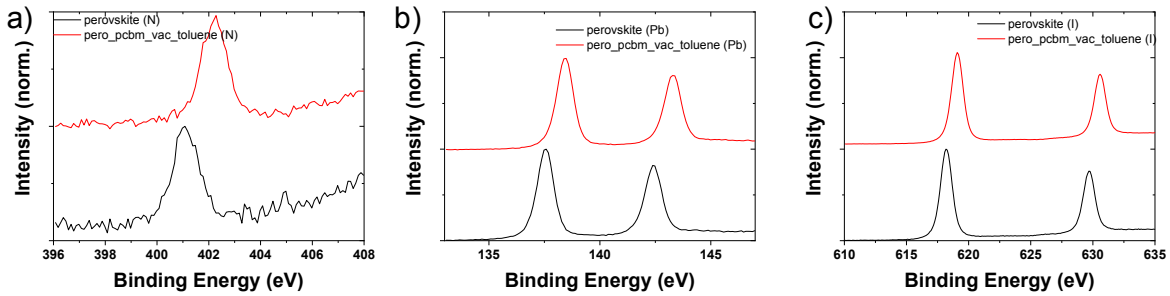

Supplementary Figure 21. High-resolution XPS spectra of pristine perovskite and perovskite after being maintained under vacuum as well as after removal of PCBM.

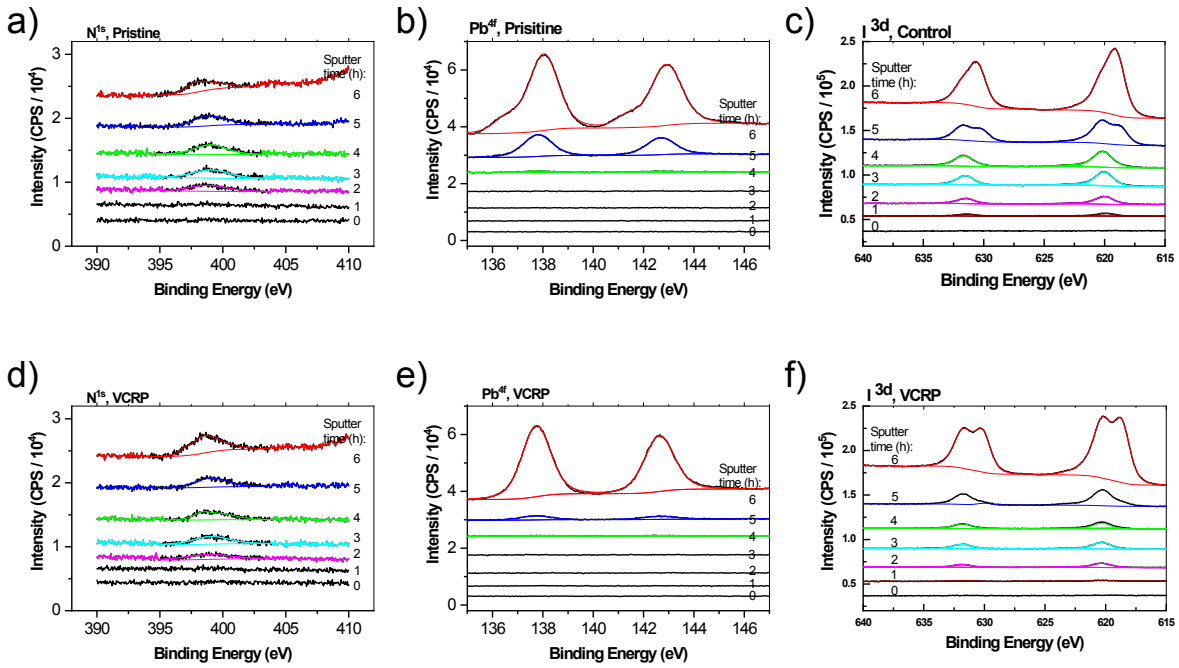

Supplementary Figure 22. (a-c). XPS depth profiles of pristine perovskite/PCBM and (d-f) VCRP-processed redeposited perovskite/PCBM.

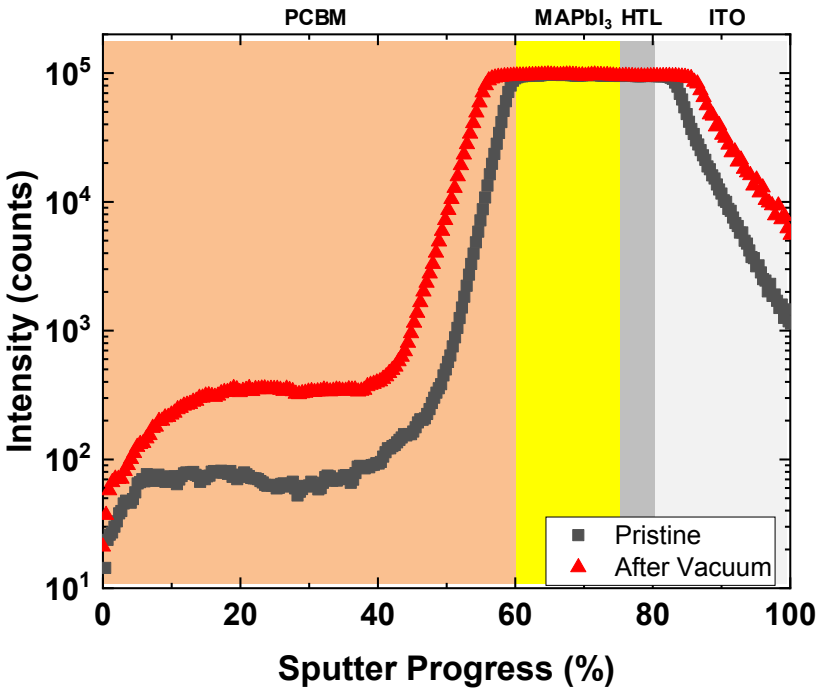

Supplementary Figure 23. I^- components of the pristine sample and vacuum cured samples of ITO/PTAA/PFN/perovskite/PCBM measured by ToF-SIMS.

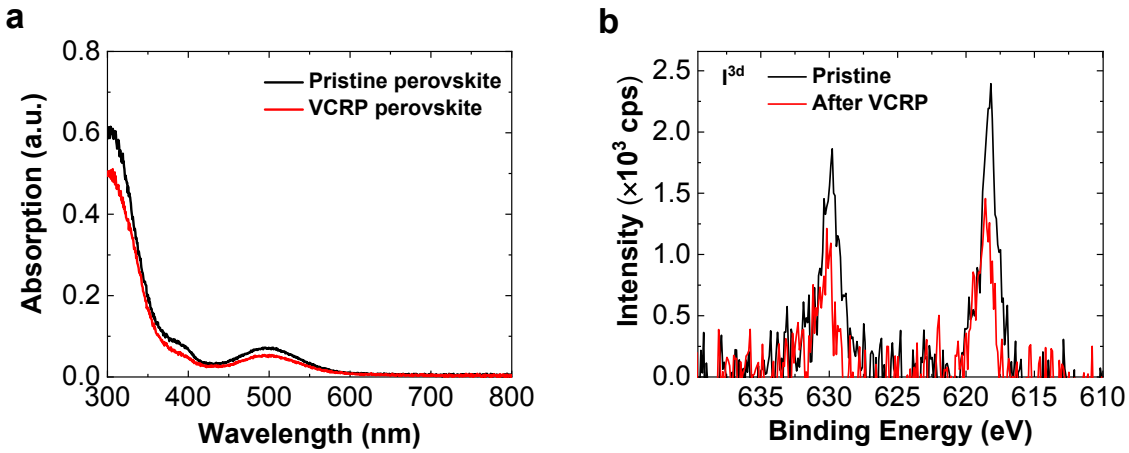

Supplementary Figure 24. Iodine diffusion of perovskite layers. (a) absorbance of iodine extracted from $MAPbI_3$ films (pristine and VCRP processed sample) immersed in toluene, and (b) I^{3d} XPS spectra on PCBM surfaces of the aged pristine and VCRP processed PeSCs.

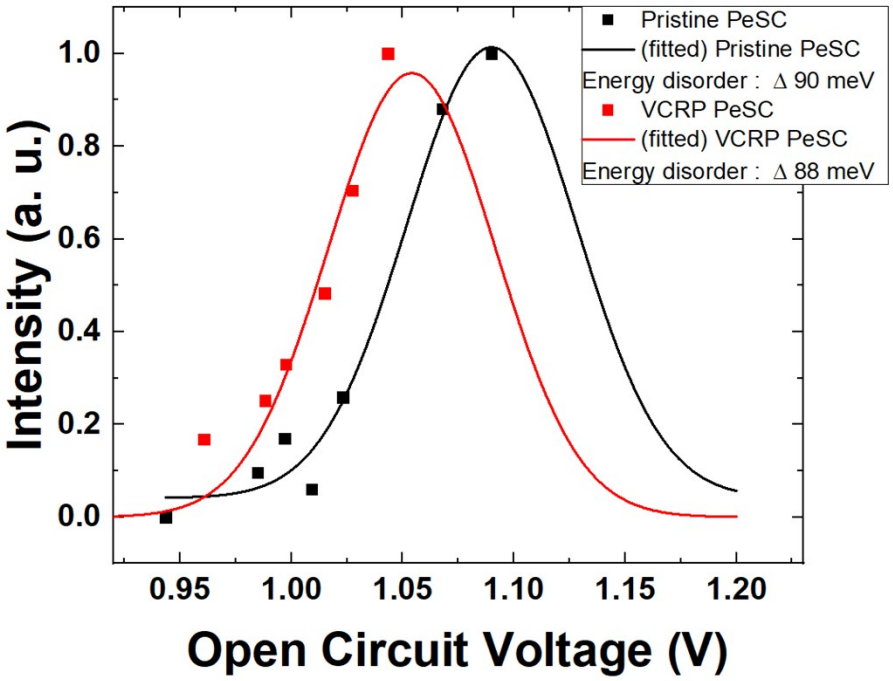

Supplementary Figure 25. Energetic disorder of pristine and VCRP PeSCs.

Supplementary Table 1. Summary of the performance characteristics of PeSCs before and after the aging process.

Treatment #	Initial Aging time	V_{oc} [V]	J_{sc} [mA cm^{-2}]	FF	PCE [%]	Decay/hour (%/h)
1st	Initial	1.1	20.44	0.75	16.91	26.7
	21	1.07	15.67	0.67	11.31	
2nd	Initial	1.09	19.92	0.69	15.10	16.9
	15	1.09	16.39	0.71	12.57	
3rd	Initial	1.09	18.63	0.73	14.77	18.0
	62	1.08	7.61	0.43	3.56	
4th	Initial	1.07	17.41	0.69	12.92	5.3
	123	1.06	11.39	0.53	6.35	

Supplementary Table 2. Summary of the performance characteristics of pristine and VCRP PeSCs.

Device	Sweep direction	V_{oc} [V]	J_{sc} [mA cm^{-2}]	FF	PCE [%]
Pristine	FWD	1.10	20.89	0.79	18.23
	REV	1.10	20.87	0.79	18.21
VCRP	FWD	1.11	20.92	0.77	17.74
	REV	1.11	20.86	0.77	17.84

Supplementary Table 3. Summary of the performance characteristics of VCRP PeSCs before and after MPPT for 1000 hours.

Device	Sweep direction	V_{oc} [V]	J_{sc} [mA cm^{-2}]	FF	PCE [%]
Pristine	FWD	1.06	19.78	0.73	15.22
	REV	1.07	19.63	0.78	16.34
After 1000 hr aging	FWD	1.04	17.82	0.68	12.49
	REV	1.04	18.01	0.71	13.19
After 1000 hr aging & re-deposition	FWD	1.06	20.31	0.61	13.06
	REV	1.05	20.44	0.63	13.65

Supplementary Table 4. Summary of the performance characteristics of VCRP PeSCs before and after thermal aging for 1000 hours.

Device	Sweep direction	V_{oc} [V]	J_{sc} [mA cm^{-2}]	FF	PCE [%]
Pristine	FWD	1.08	20.79	0.76	17.11
	REV	1.08	20.68	0.77	17.21
After 1000 hr thermal aging	FWD	1.10	21.78	0.63	15.18
	REV	1.10	21.75	0.65	15.61

Supplementary Table 5. Summary of the 110 peak position and FWHM of the perovskite layer.

Sample	Peak 1 Å	FWHM Å
Perovskite	1.00	0.050
Perovskite/PCBM	1.00	0.053
Perovskite/PCBM/vacuum	0.98	0.028
Perovskite/PCBM/vacuum/toluene	0.98	0.038

Supplementary Table 6. Atomic ratio determined from high-resolution XPS spectra of pristine perovskite and perovskite after being maintained under vacuum as well as after removal of PCBM.

Sample	Pb : N : I Ratio		
	Pb/Pb	N/Pb	I/Pb
Perovskite	1.00	0.84	2.83
Perovskite after vacuum contained than remove PCBM	1.00	1.04	3.30

References

1. M. Alsari, O. Bikondoa, J. Bishop, M. Abdi-Jalebi, L. Y. Ozer, M. Hampton, P. Thompson, M. T. Hörantner, S. Mahesh, C. Greenland, J. E. Macdonald, G. Palmisano, H. J. Snaith, D. G. Lidzey, S. D. Stranks, R. H. Friend and S. Lilliu, *Energy Environ. Sci.*, 2018, **11**, 383-393.
2. S. Lilliu, J. Griffin, A. T. Barrows, M. Alsari, B. Curzadd, T. G. Dane, O. Bikondoa, J. E. Macdonald and D. G. Lidzey, *CrystEngComm*, 2016, **18**, 5448-5455.
3. S. Lilliu, T. G. Dane, M. Alsari, J. Griffin, A. T. Barrows, M. S. Dahlem, R. H. Friend, D. G. Lidzey and J. E. Macdonald, *Adv. Funct. Mater.*, 2016, **26**, 8221-8230.
4. Grazing Incidence X-ray Scattering and Diffraction on Thin Films, https://www-ssrl.slac.stanford.edu/materialscatter/scatter-grazing.html).
5. X-ray Mass Coefficient of Pb, https://physics.nist.gov/PhysRefData/XrayMassCoef/ElemTab/z82.html).